

---

# The combination of micron and nanotopography by H<sub>2</sub>SO<sub>4</sub>/H<sub>2</sub>O<sub>2</sub> treatment and its effects on osteoblast-specific gene expression of hMSCs

---

Gustavo Mendonça,<sup>1,2,3</sup> Daniela B. S. Mendonça,<sup>1,2</sup> Francisco J. L. Aragão,<sup>1,4</sup> Lyndon F. Cooper<sup>2</sup>

<sup>1</sup>Universidade Católica de Brasília, Pós-Graduação em Ciências Genômicas e Biotecnologia, SGAN Quadra 916, Módulo B, Av. W5 Norte 70.790-160-Asa Norte, Brasília/DF, Brazil

<sup>2</sup>Bone Biology and Implant Therapy Laboratory, Department of Prosthodontics, University of North Carolina at Chapel Hill, 404 Brauer Hall, CB #7450, Chapel Hill, North Carolina 27511

<sup>3</sup>Universidade Católica de Brasília, Curso de Odontologia, QS 07, Lt 01-EPCT, Taguatinga/DF, Brazil

<sup>4</sup>Embrapa Recursos Genéticos e Biotecnologia, Laboratório de Introdução e Expressão de Genes, PqEB W5 Norte 70770-900, Brasília/DF, Brazil

Received 17 February 2009; revised 14 September 2009; accepted 2 October 2009

Published online 2 February 2010 in Wiley InterScience (www.interscience.wiley.com). DOI: 10.1002/jbm.a.32701

**Abstract:** H<sub>2</sub>SO<sub>4</sub>/H<sub>2</sub>O<sub>2</sub> treatment of titanium implants imparts nanofeatures to the surface and alters the osteoblast response. The aim of this study was to evaluate the effect of H<sub>2</sub>SO<sub>4</sub>/H<sub>2</sub>O<sub>2</sub> treatment of commercially pure Titanium (cpTi) surfaces on gene expression of human mesenchymal stem cells (hMSCs) differentiated into osteoblasts. Commercially pure grade IV titanium disks (20.0 mm × 1.0 mm) were polished or polished and subsequently treated by grit blasting or grit-blasting/acid etching with an H<sub>2</sub>SO<sub>4</sub>/H<sub>2</sub>O<sub>2</sub> solution. The surfaces were divided into three groups: smooth (S), grit-blasted (Gb), and nanostructured: grit-blasted/acid etched (Nano). Surfaces were examined by scanning electron microscopy and atomic force microscopy. hMSCs were grown on the disks. The data points analyzed were at 3, 7, 14, and 28 days. Real-time PCR was used to measure the mRNA levels of *ALP*, *BSP*, *Runx2*, *OCN*, *OPN*, and *OSX*. The house-

keeping gene *GAPDH* was used as a control. Descriptive statistics were calculated using Microsoft Excel. *T*-test was performed for comparison of mRNA levels when compared with S surfaces ( $p < 0.05$ ). All osteoblast-specific genes were regulated in surface-dependent patterns and most of them were upregulated on the Nano surfaces. *Runx2* and *OSX* mRNAs were more than threefold upregulated at days 14 and 28 on Nano. Higher levels for *ALP* (38-fold), *BSP* (76-fold), and *OCN* (3-fold) were also observed on the Nano surfaces. A grit-blasted surface imparted with nanofeatures by H<sub>2</sub>SO<sub>4</sub>/H<sub>2</sub>O<sub>2</sub> treatment affected adherent cell bone-specific gene expression. © 2010 Wiley Periodicals, Inc. *J Biomed Mater Res 94A*: 169–179, 2010

**Key words:** nanotopography; peroxidation; dental implant; surface treatment; bone regeneration

---

## INTRODUCTION

Implant surface technology has evolved in the last decade and focused on developing new surfaces capable of supporting the osseointegration process even in compromised patients. In the early 1980s, the main clinical advantage of osseointegration was the predictable clinical result that occurred when an osseous interface was reproducibly formed and maintained at

the titanium surface of load-bearing dental implants.<sup>1</sup> This outcome is much more predictable in patients with a more dense bone type (bone types 1–3), and less predictable in poor quality bone (type 4).<sup>2,3</sup> Some selected patient populations (e.g., smokers, diabetics) show reduced osseointegration success.<sup>3–5</sup> The cause of these failures, while not precisely determined, was largely attributed to a failure in bone formation in support of osseointegration. Challenging osseointegration with new protocols such as immediate placement and immediate loading may also require further control of bone formation and osseointegration.<sup>6</sup>

The implant surface plays an important role affecting the rate and extent of osseointegration.<sup>7–11</sup> Many studies have given insight into the osseointegration process, and it is now described at both the histological level and at the cellular level.<sup>12</sup> The adhesion of a fibrin blood clot allows the implant surface being colonized

Correspondence to: G. Mendonça; e-mail: mendonca@ucb.br or L. F. Cooper; e-mail: lyndon\_cooper@dentistry.unc.edu

Contract grant sponsors: Coordenação de Aperfeiçoamento de Pessoal de Nível Superior (CAPES), Conselho Nacional de Desenvolvimento Científico e Tecnológico (CNPq), UNC-Astratech Fellowship

by blood-derived and mesenchymal stem cells.<sup>13–15</sup> These cell populations lead to elaboration and modification of the tissue/implant interface resulting in bone formation in direct contact with the implant surface. Osseointegration can also be considered to play an important role, specially when a more rapid and complete bone formation is achieved and is also directly influenced by the implant surface.<sup>7</sup> The effect of implant surface and how it affects direct bone contact, how rapidly this bone accrual occurs, and the mechanical nature of the bone/implant connection is influenced by the nature of the implant surface itself.<sup>16</sup>

Early investigations revealed the biocompatible nature of the commercial pure Titanium (cpTi) implant,<sup>17</sup> and the importance of the implant surface was brought into consideration in this complex process of osseointegration in a number of different ways. Several investigations at the cellular and molecular levels have contributed to defining cellular responses to titanium as “compatible” and advantageous. Subsequently, experiments with surface topography encouraged new considerations of improvements in bone formation at the implant surface. In the early 1990s, an important role for surface microtopography was advocated.<sup>18</sup> More recently, several investigations have implicated implant surface nanoscale topographic control of cell behavior or the combination of micro and nanofeatures to improve the osseointegration process<sup>19–28</sup> and influence the differentiation of mesenchymal stem cells into osteoblasts.<sup>27</sup>

There exist numerous ways that the implant surface can be modified; micron-scale and nanoscale features can be added to these surfaces in combination. Chemical treatment [Peroxidation ( $H_2O_2$ ) or acid oxidation, such as hydrofluoric acid] of titanium surfaces to expose reactive groups on the material surface and create different topographies is one of the methods that can be used.<sup>8,9,18,20,21,23,28</sup> Both chemical and topography changes are imparted.  $H_2O_2$  with acid etching has been shown to create novel nanostructures of amorphous titanium oxide on the implant surface.<sup>28–30</sup>

Based on the hypothesis that nanostructured surfaces can modulate initial osteoinductive responses of cells to increase bone-specific gene expression, the aim of this study was to evaluate the gene expression of human mesenchymal stem cells (hMSCs) differentiated into osteoblasts and cultured on cpTi disks modified with either micron or micron with superimposed nanoscale features.

## MATERIALS AND METHODS

### Surfaces preparation

Commercially pure grade IV titanium disks (20.0 mm × 1.0 mm) were prepared. All the disks were polished using

Si carbide papers starting from grade 320, 400, to 600 grits. Subsequently, one group of disks were grit-blasted with 100- $\mu$ m aluminum oxide particles and sonicated three times in water for 15 min each to clean, followed by immersion in 50/50 v/v % solution of 30%  $H_2O_2$  and 2N  $H_2SO_4$  (Fisher Scientific, Pittsburgh, PA) for 2 h.<sup>8,28,31</sup> Following treatment with  $H_2SO_4/H_2O_2$  solution, the substrates were sonicated three times in ultrapure deionized (DI) water (resistivity 1/4 8.2MO, pH1/4 6.82; Millipore), and then three times in 70% ethanol, before drying under the hood (samples prepared in this manner are hereafter referred to as “Nano”). Another set of disks was polished only up to 600 grits and composed the smooth (S) group. These disks were sonicated three times in water for 15 min each to clean, and then it was passivated with 30%  $HNO_3$  for 5 min. A third group was composed of disks that were polished and grit-blasted, cleaned and passivated with 30%  $HNO_3$  for 5 min [these disks composed the grit-blasted (Gb) group]. The sequence for disks preparation is shown in Table I.

### Surfaces analysis

The disk surfaces were examined by a high-resolution scanning electron microscope [SEM; field emission SEM (FEG-SEM), Hitachi S-4700, Tokyo, Japan] and atomic force microscopy (AFM; Nanoscope IIIA AFM; Digital Instruments, Santa Barbara, CA). Observations were made at three randomly selected points on the disk surfaces, and average values were calculated.

### Cell culture

hMSCs P2 were purchased (Lonza) and cultured in accordance with published protocols.<sup>32</sup> Growth media included Dulbecco’s modified eagle medium low glucose (LG-DMEM) (Gibco) supplemented with 10% fetal bovine serum (FBS) and antibiotic/antimycotic (penicillin/streptomycin/amphotericin B; Sigma). Osteogenic media includes LG-DMEM (Gibco, #11885) supplemented with 10% FBS and antibiotic/antimycotic and the osteogenic supplements 100 nM dexamethasone (Sigma), 10 mM glycerophosphate (Sigma, G9891), and 0.2 mM ascorbic acid (Sigma). Passage 2 cells were plated at low density and grown until nearly confluent. Cells were passaged onto prepared titanium disks using 100,000 cells in 250  $\mu$ L of growth media. The formed meniscus was left undisturbed to permit cell attachment over 4 h and subsequently additional growth media was applied. Following overnight incubation, cultures were carefully rinsed and osteogenic media was placed in culture dishes. This represented the starting time point ( $T = 0$ ). The osteogenic media was replaced every third day. Disks with adherent cell and forming tissue layers were collected on days 3, 7, 14, and 28.

### RNA isolation and analysis

For evaluation of mRNA expression in cells adherent to titanium disks, disks were removed from the culture

**TABLE I**  
Surfaces Preparation

	Polishing with Si Carbide Papers	Grit-Blasting with 100- $\mu$ m Aluminum Oxide Particles	Passivated with 30% HNO <sub>3</sub>	Immersion H <sub>2</sub> O <sub>2</sub> /H <sub>2</sub> SO <sub>4</sub> Solution
Smooth (S)	Yes		Yes	
Grit-blasted (Gb)	Yes	Yes	Yes	
Acid-etched (Nano)	Yes	Yes		Yes

dishes and rinsed twice with cold phosphate-buffered saline. Adherent cells on each disk were lysed using Trizol (Invitrogen, Carlsbad, CA) and lysates were collected by pipetting and centrifugation. Total RNA in the cell lysates was isolated according to the manufacturer's protocol and collected by ethanol precipitation. Total RNA was quantified using UV spectrophotometry. From each total RNA sample, cDNA was generated using RT<sup>2</sup> First Strand Kit reverse transcriptase (SABiosciences, Frederick, MD) in a standard 20  $\mu$ L reaction using 1  $\mu$ g of the total RNA. All cDNAs were subjected to polymerase chain reaction (PCR) for *GAPDH* mRNA as a test of RNA integrity and cDNA synthesis. Subsequently, equal volumes of cDNA were used to program real-time PCR reactions specific for mRNAs encoding *ALP*, *BSP*, *Runx2*, *OCN*, *OPN*, and *OSX*. Reactions were performed using a customized RT<sup>2</sup> Profiler<sup>TM</sup> PCR Arrays (CAPH-0398) (SABiosciences) and ther-

mocycling in an ABI 7200 real-time thermocycler (Applied Biosystems, Foster City, CA). Relative mRNA abundance was determined by the 2<sup>- $\Delta\Delta$ Ct</sup> method and reported as fold induction. *GAPDH* abundance was used for normalization.<sup>33</sup> The data points were analyzed at 3, 7, 14, and 28 days.

### Statistical analyses

Descriptive statistics were calculated using SPSS. The roughness parameter ( $S_a$ ) was compared by one-way ANOVA followed by Tukey Test. For the gene expression analysis, descriptive statistics were calculated using Microsoft Excel. *T*-test was performed for the comparison of mRNA levels when compared with S surfaces.<sup>34,35</sup> For all statistical analysis, significance level was set at  $p < 0.05$ .

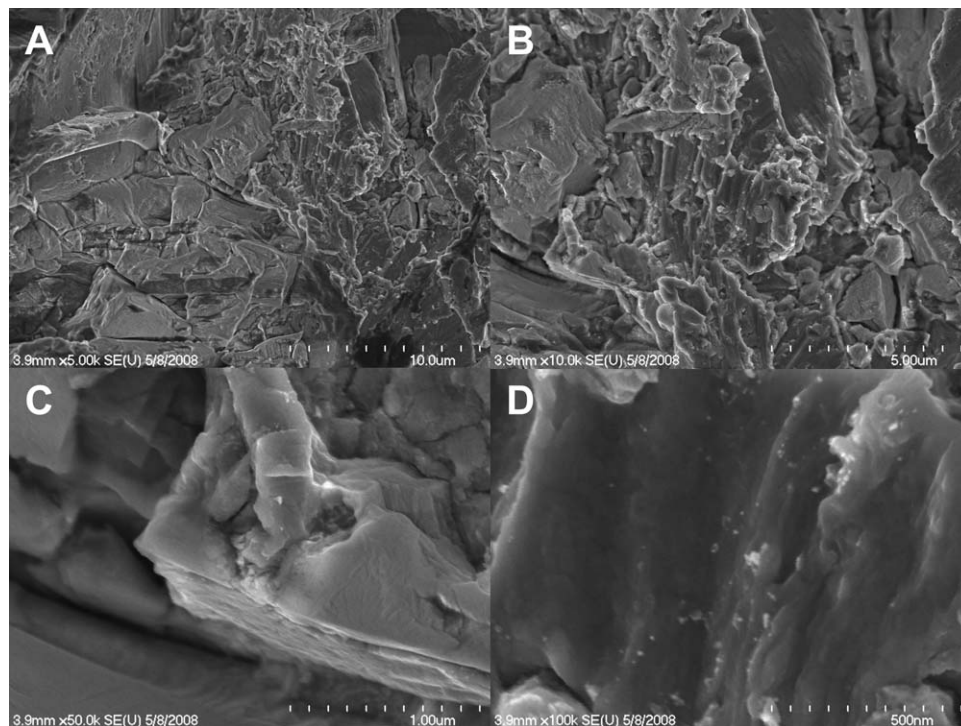


**Figure 1.** Scanning electron micrographs of the surface prepared by grit blasting with 100- $\mu$ m Al<sub>2</sub>O<sub>3</sub> particles—Grit-blasted surface (Gb). In (A) and (B), the surface is shown at low magnification ( $\times 5000$  and  $\times 10,000$ , respectively) and demonstrates the micron-scale features on the surface created by grit blasting. In (C) and (D), the surface is shown at a higher magnification ( $\times 50,000$  and  $\times 100,000$ , respectively) and demonstrates the relative absence of nanoscale features. Scale bar = 10  $\mu$ m (A), 5  $\mu$ m (B) 1  $\mu$ m (C), and 500 nm (D).

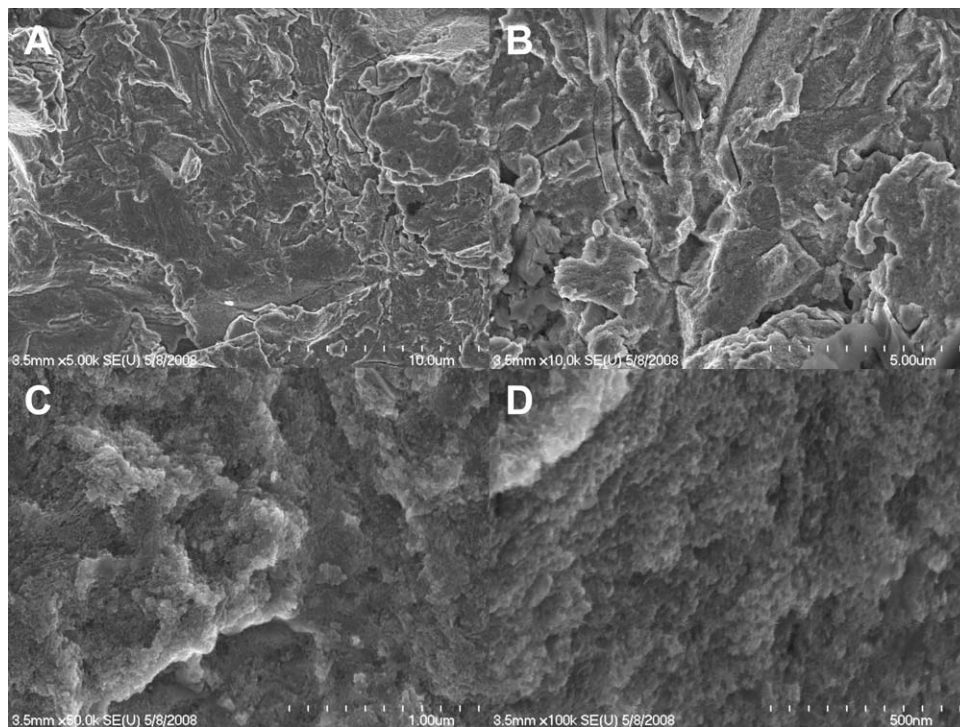


**Figure 2.** Scanning electron micrographs of the surface prepared by grit blasting with 100- $\mu\text{m}$   $\text{Al}_2\text{O}_3$  particles followed by  $\text{H}_2\text{SO}_4/\text{H}_2\text{O}_2$  treatment—nanostructured (Nano) surface. In (A) and (B), the surface is shown at low magnification ( $\times 5000$  and  $\times 10,000$ , respectively) and demonstrates the micron-scale features on the surface created by the grit blasting process. In (C) and (D), the surface is shown at a higher magnification ( $\times 50,000$  and  $\times 100,000$ , respectively) and it shows nanofeatures imparted to the surface due to the  $\text{H}_2\text{SO}_4/\text{H}_2\text{O}_2$  oxidative treatment. Scale bar = 10  $\mu\text{m}$  (A), 5  $\mu\text{m}$  (B), 1  $\mu\text{m}$  (C), and 500 nm (D).

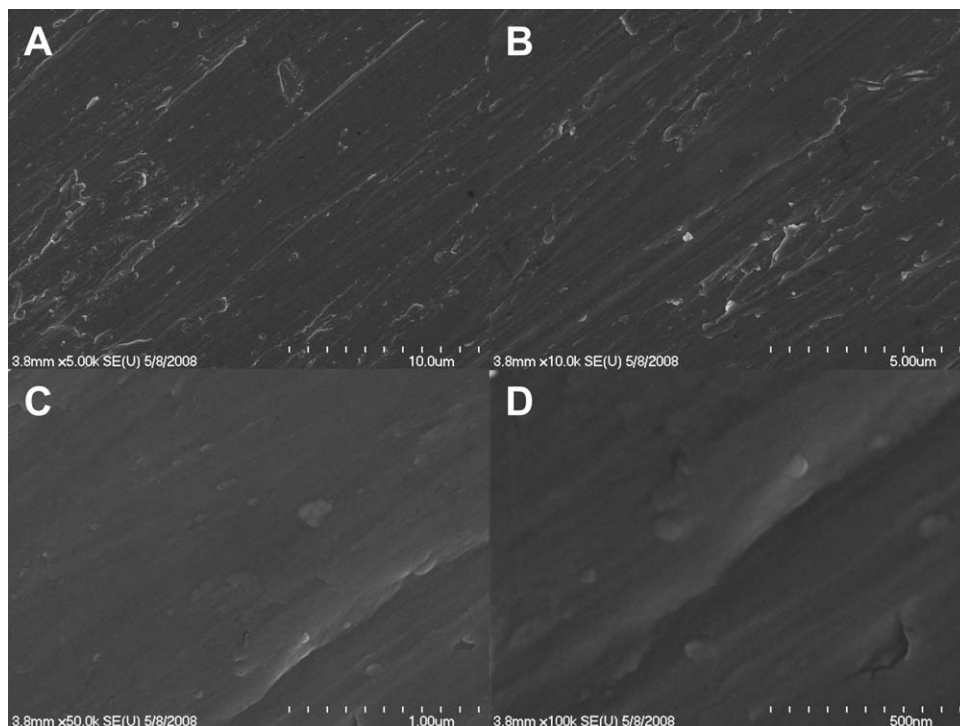


**Figure 3.** Scanning electron micrographs of the smooth (S) surface. In (A) and (B), the surface is shown at low magnification ( $\times 5000$  and  $\times 10,000$ , respectively) and it is rather flat when compared with the other surfaces. In (C) and (D), the surface is shown at a higher magnification ( $\times 50,000$  and  $\times 100,000$ ) and demonstrates the relative absence of nanoscale features. Scale bar = 10  $\mu\text{m}$  (A), 5  $\mu\text{m}$  (B), 1  $\mu\text{m}$  (C), and 500 nm (D).

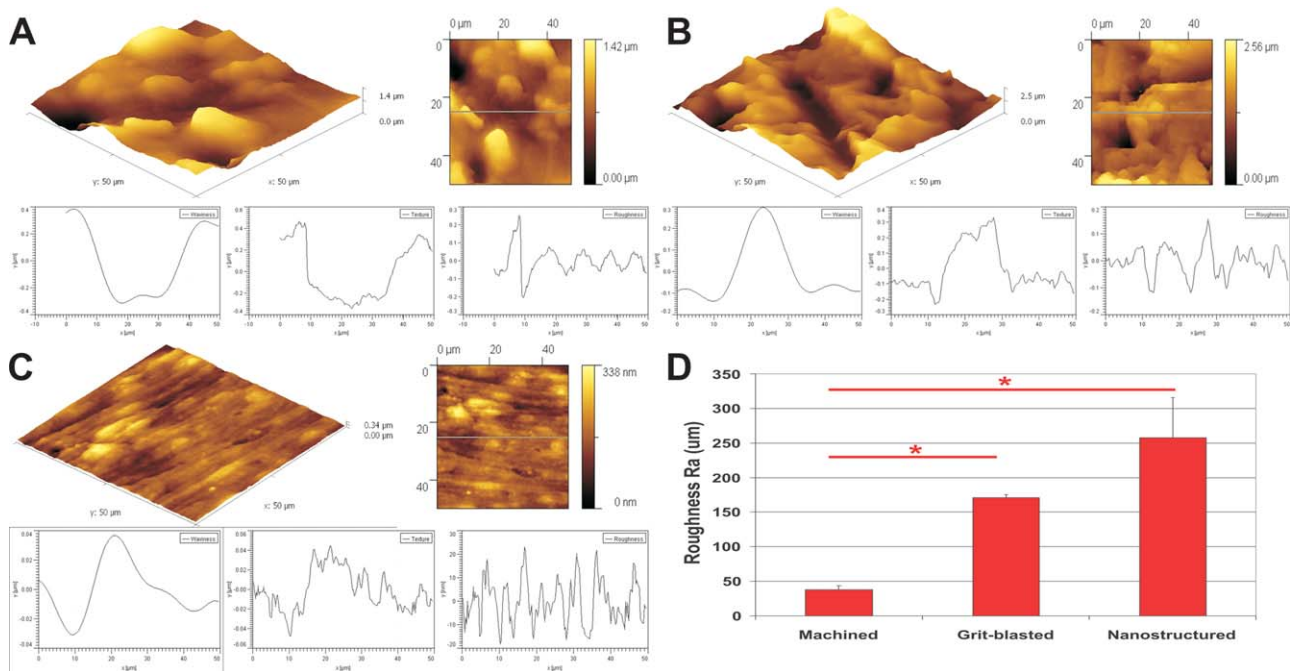


**Figure 4.** AFM images of the evaluated surfaces: (A) grit-blasted, (B) nanostructured, and (C) smooth. The images in (A)–(C) show the 3D (left side) and 2D (right side) images for each surface. The graphs 1, 2, and 3 for each surface show the waviness, texture, and roughness, respectively, and were obtained from the horizontal lines in the 2D images. In (D), the roughness ( $R_a$ ) of each surface obtained from the AFM is depicted. \*Statistically significant difference ( $p < 0.05$ ). [Color figure can be viewed in the online issue, which is available at [www.interscience.wiley.com](http://www.interscience.wiley.com).]

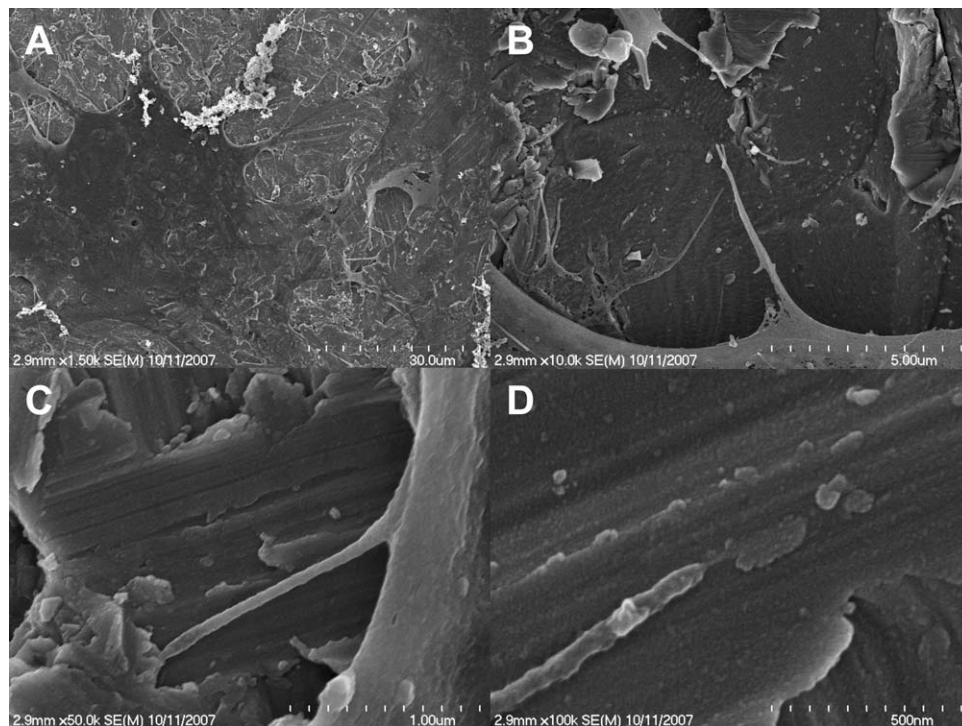


**Figure 5.** Scanning electron micrographs of hMSCs growing on the Smooth surface. In (A) and (B), the cell/surface interaction is shown at low magnification ( $\times 1500$  and  $\times 10,000$ , respectively). In (B; at  $\times 10,000$ ), a little fillopodia can be observed. In (C) and (D), the cell/surface interaction is shown at a higher magnification ( $\times 50,000$  and  $\times 100,000$ , respectively) and the interaction between the cells and the surface is observed by the extended fillopodia. Scale bar = 30 μm (A), 5 μm (B), 1 μm (C), and 500 nm (D).

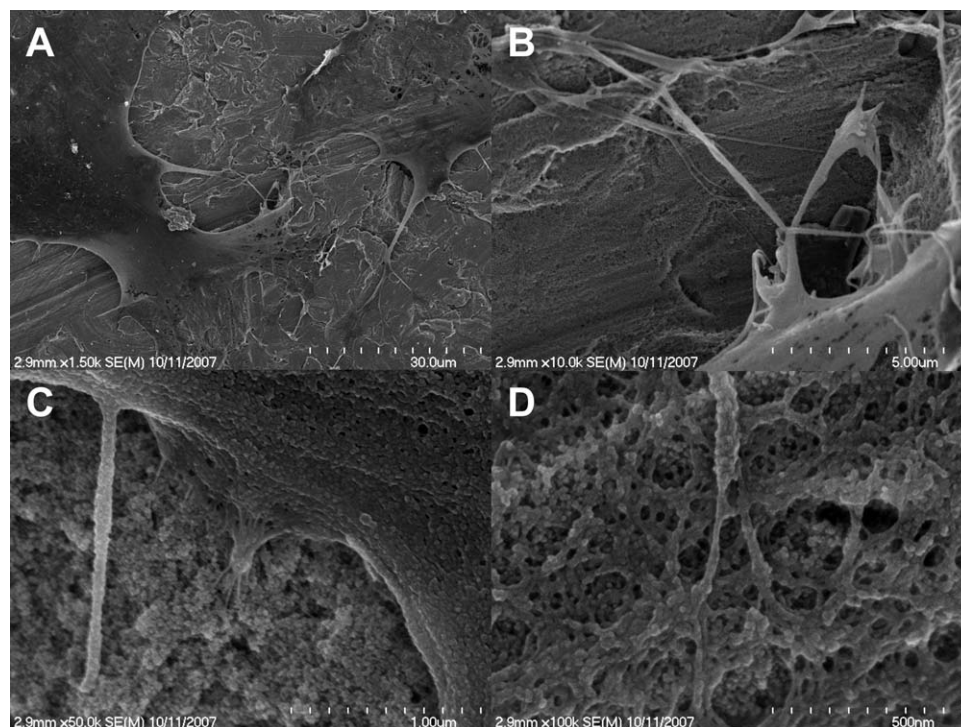


**Figure 6.** Scanning electron micrographs of hMSCs growing on the Nano (Grit-blasted/Oxidative treatment) surface. In (A) and (B), the cell/surface interaction is shown at low magnification ( $\times 1500$  and  $\times 10,000$ , respectively). At  $\times 1500$  magnification, no changes are observed when compared with Figure 5; however, (B) at  $\times 10,000$ , an increased lamellipodia is observed on Nano. In (C) and (D), the cell/surface interaction is shown at a higher magnification ( $\times 50,000$  and  $\times 100,000$ , respectively) demonstrating the interaction between the cells and the nanofeatures of the surface. The 20–40 nm features produced by the oxidative treatment are interactive points for lamellipodia of spreading cells. Scale bar = 30  $\mu\text{m}$  (A), 5  $\mu\text{m}$  (B), 1  $\mu\text{m}$  (C), and 500 nm (D).

## RESULTS

### Surface analysis

The surfaces in this study not only presented different characteristics related to the nanoscale level but also included microscale topographic differences. At low resolution, SEMs revealed the conservation of micron-scale features between the two grit-blasted surfaces (GB and Nano) (Figs. 1 and 2) and the absence of similar micron-scale features for the S surfaces (Fig. 3). At high resolution, the presence of discrete 20–30 nm nanofeatures on the  $\text{H}_2\text{SO}_4\text{-}/\text{H}_2\text{O}_2$ -treated surfaces (Fig. 2) were observed. A little or no nanoscale features on the grit-blasted only (Gb group) or on the S group (smooth surface) (Figs. 1 and 3) were observed.

The measurement of surface parameters showed a difference among the three prepared surfaces (Fig. 4). The  $S_a$  roughness parameter confirmed a smoother surface for the S group, which was polished (600-grit sandpaper). The GB and Nano groups presented higher  $S_a$  values.  $S_a$  values for the GB group was 160 nm. The highest  $S_a$  values (260 nm) were in the Nano group and were due to the subsequent acid etch treatment following the grit blasting (Fig. 4). The waviness

of both GB and Nano surfaces were similar and much higher than the S surface (Fig. 4).

Cells were successfully grown and expanded on all surfaces. Cell formed multilayer cultures. Retrac-

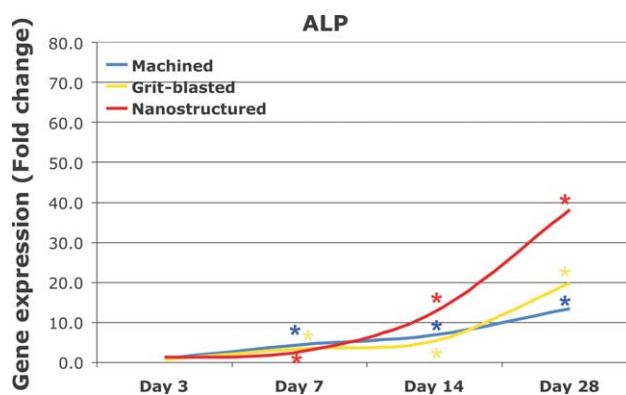


**Figure 7.** Adherent hMSCs ALP mRNA expression. Expression levels (fold change) are compared among all surfaces. Total RNA was isolated from cells at 3, 7, 14, and 28 days of culture on machined, grit-blasted, and nanostructured titanium disks. The results are shown as fold change ( $2^{-\Delta\Delta\text{Ct}}$  method, baseline = day 3 cells on Machined surface). \*Statistically significant difference when compared with baseline ( $p < 0.05$ ). [Color figure can be viewed in the online issue, which is available at [www.interscience.wiley.com](http://www.interscience.wiley.com).]

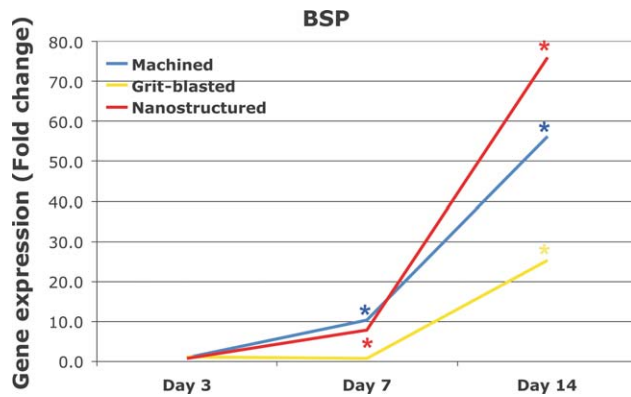


**Figure 8.** Adherent hMSCs *BSP* mRNA expression. Expression levels (fold change) are compared among all surfaces. Total RNA was isolated from cells at 3, 7, and 14 days of culture on machined, grit-blasted, and nanostructured titanium disks. The results are shown as fold change ( $2^{-\Delta\Delta C_t}$  method, baseline = day 3 cells on Machined surface). \*Statistically significant difference when compared with baseline ( $p < 0.05$ ). [Color figure can be viewed in the online issue, which is available at [www.interscience.wiley.com](http://www.interscience.wiley.com).]

tion from the disks was not observed. From the cultures established with 100,000 cells, there were sufficient numbers of cells present after 3, 7, 14, and 28 days for isolation of total RNA ( $>5 \mu\text{g}$  of total RNA) to perform the arrayed real-time PCR reactions.

Figures 5 and 6 show hMSCs adhered to S and Nano surfaces after 24 h. At  $1500\times$  magnification, hMSCs on both surfaces appeared similar; however, at  $10,000\times$  increased filopodia were observed for hMSCs adhered to Nano surfaces. At  $50,000\times$  and  $100,000\times$ , the interaction between the cells and the nanofeatures of the surface is evident. The differen-

ces in spreading, adhesion, and proliferation of cells between the surfaces was not observed and was not in the scope of this investigation.

The surface-specific gene regulation was observed for the six studied genes (Figs. 7–12). One general observation was that early differences among the surfaces (days 3 or 7) were often of lower magnitude than differences observed at 14 and 28 days. At day 3, no statistical differences were found in gene expression among the surface groups. Another observation was that the Nano group presented, at day 7, an expression pattern similar to S for all genes. After 14 days, Nano presented a marked increase when compared with GB and S.

*ALP* mRNAs levels (Fig. 7) were greatest in hMSCs on Nano surfaces. At days 14 and 28, *ALP* mRNA was 12-fold and 38-fold upregulated, respectively, when compared with an expression for S (6- and 13-fold at days 14 and 28, respectively) and GB (5- and 19-fold at days 14 and 28, respectively) surfaces. *BSP*-relative mRNA expression (Fig. 8) was similarly upregulated for both GB and Nano at day 7 (10-fold increase). At day 14, the expression levels for S, GB, and Nano were 25-, 55-, and 80-fold, respectively. *OPN* mRNA levels (Fig. 9) were constant for S throughout the 28 days period of the experiment. Increase of *OPN* was observed in hMSCs on both GB and Nano surfaces. At day 28, the *OPN* relative expression level in cells on GB and Nano surfaces were more than 50-fold increase on both surfaces.

The levels of *OCN* mRNA expression (Fig. 10) were modestly increased ( $\sim 3$ -fold) for S and Nano at day 14 and kept the same rate for Nano at day 28.

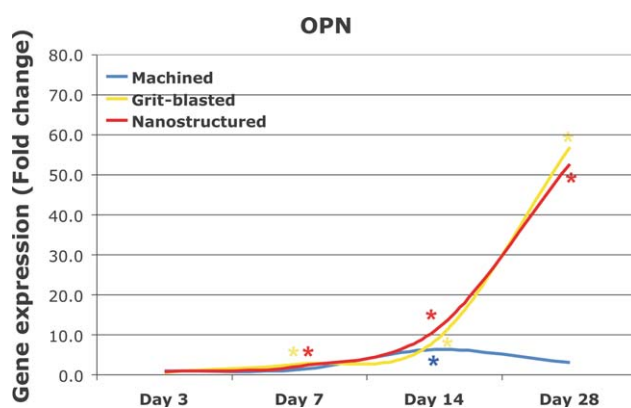


**Figure 9.** Adherent hMSCs *OPN* mRNA expression. Expression levels (fold change) are compared among all surfaces. Total RNA was isolated from cells at 3, 7, 14, and 28 days of culture on machined, grit-blasted, and nanostructured titanium disks. The results are shown as fold change ( $2^{-\Delta\Delta C_t}$  method, baseline = day 3 cells on Machined surface). \*Statistically significant difference when compared with baseline ( $p < 0.05$ ). [Color figure can be viewed in the online issue, which is available at [www.interscience.wiley.com](http://www.interscience.wiley.com).]

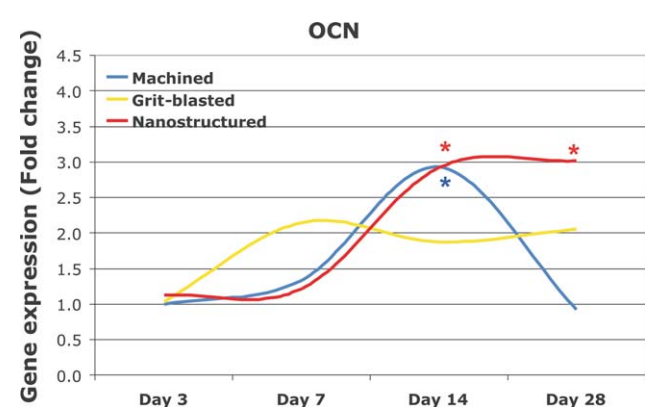


**Figure 10.** Adherent hMSCs *OCN* mRNA expression. Expression levels (fold change) are compared among all surfaces. Total RNA was isolated from cells at 3, 7, 14, and 28 days of culture on machined, grit-blasted, and nanostructured titanium disks. The results are shown as fold change ( $2^{-\Delta\Delta C_t}$  method, baseline = day 3 cells on Machined surface). \*Statistically significant difference when compared with baseline ( $p < 0.05$ ). [Color figure can be viewed in the online issue, which is available at [www.interscience.wiley.com](http://www.interscience.wiley.com).]

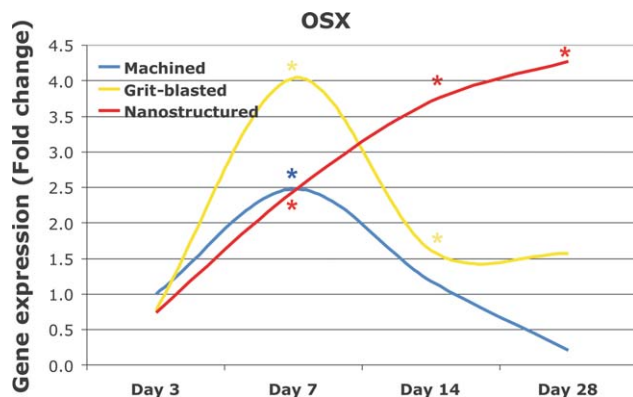


**Figure 11.** Adherent hMSCs OSX mRNA expression. Expression levels (fold change) are compared among all surfaces. Total RNA was isolated from cells at 3, 7, 14, and 28 days of culture on machined, grit-blasted, and nanostructured titanium disks. The results are shown as fold change ( $2^{-\Delta\Delta C_t}$  method, baseline = day 3 cells on Machined surface). \*Statistically significant difference when compared with baseline ( $p < 0.05$ ). [Color figure can be viewed in the online issue, which is available at [www.interscience.wiley.com](http://www.interscience.wiley.com).]

The levels of OCN mRNA for S dropped close to the baseline level at 28 days. For GB, the OCN mRNA relative levels reached a twofold increase at 7 days and kept constant throughout the experiment.

OSX mRNA (a key transcription factor for osteoblast differentiation) expression levels (Fig. 11) were 2.5-, 3.5-, and 4- fold upregulated at days 7, 14 and 28 in cells on the Nano surfaces. For the S surface, OSX levels reached 2.5-fold increase at day 7 and then decreased to baseline. OSX expression levels for GB reached up to fourfold at day 7, but subsequently dropped to baseline levels thereafter. The relative expression levels of *Runx2* mRNA (Fig. 12) was 3.5-fold greater for Nano at days 14 and 28. For the GB surface, it varied to 2.5-fold over same period. The *Runx2* expression levels for S surface increased twofold at day 14.

## DISCUSSION

The importance of endosseous dental implant surface topography has been demonstrated in many studies,<sup>18,36,37</sup> but until the late 1990s, investigation focused on micron-scale modifications.<sup>18,36</sup> More recently, the focus has shifted to the nanoscale level.<sup>7,16,23,38</sup> The observation that a micron-scale rough surface prepared by grit blasting and subsequent hydrofluoric acid (HF) treatment presented a superimposed nanotopography suggested that nanoscale modifications could alter adhered cellular activity or tissue responses leading to greater osteogenesis.<sup>20,39–41</sup> In this study, 100- $\mu$ m aluminum oxide par-

ticles were used to create the microtopography by grit blasting. Subsequent acid etching and peroxidation with a  $H_2SO_4/H_2O_2$  treatment created a superimposed nanotopography confirming previous similar effects.<sup>8,31</sup> The modification of the  $H_2SO_4$  concentration from 37N to 2N resulted in an observable alteration of the nanofeatures present on the surface when compared with previously published studies using peroxidation.<sup>8,28,31</sup> The presence of nanoscale features, as demonstrated by SEM and AFM, on the surfaces were evident for the Nano group when compared with S and Gb. The precise surface chemical changes that occur are not fully defined. However, all surfaces are represented of a bulk titanium oxide surface chemistry.

By observation using AFM, the changes in the  $S_a$  on the three surfaces were observed for the grit blasting process alone versus the subsequent acid etching. The waviness of the surface changed considerably from S to Gb due to the grit-blasting with 100- $\mu$ m alumina particles and increased the roughness of Gb around  $S_a = 160$  nm. The same grit-blasting step was also applied on the Nano surface, and following the acid etching, the roughness increased to  $S_a = 250$  nm. The waviness of both surfaces, Gb and Nano, are similar and due to the micron preparation (grit-blasting) of these surfaces.

Several methods may be used to create a nanoscale surface on titanium implants.<sup>8,23,29,42</sup> The use of NaOH treatment catalyzes the production of titanium nanostructures outward from the titanium surface,<sup>43</sup> creating a sodium titanate gel layer on the Ti surface.  $H_2O_2$  treatment produces a titania-gel layer.<sup>31</sup> The use of a mixture of  $H_2SO_4/H_2O_2$  has been used for deoxidation and controlled reoxidation

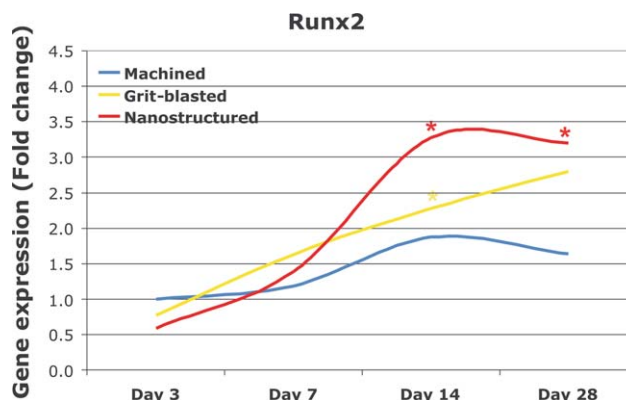


**Figure 12.** Adherent hMSCs *Runx2* mRNA expression. Expression levels (fold change) are compared among all surfaces. Total RNA was isolated from cells at 3, 7, 14, and 28 days of culture on machined, grit-blasted, and nanostructured titanium disks. The results are shown as fold change ( $2^{-\Delta\Delta C_t}$  method, baseline = day 3 cells on Machined surface). \*Statistically significant difference when compared with baseline ( $p < 0.05$ ). [Color figure can be viewed in the online issue, which is available at [www.interscience.wiley.com](http://www.interscience.wiley.com).]

of metals and creates novel nanostructures of amorphous titanium oxide on the implant surface<sup>8</sup> and improved osteoblast response.<sup>31</sup> It was found that the treatment of the implant surface with H<sub>2</sub>O<sub>2</sub>/HCl increased the adsorption of RGD peptides onto the surface followed by passivated surfaces (30% HNO<sub>3</sub>) and heat-treated surfaces.<sup>29</sup> These surface treatments also increased the mineralization in the same order. Treatment with hydrofluoric acid also creates discrete nanostructures on TiO<sub>2</sub> grit-blasted surfaces.<sup>44</sup> Titanium oxide nanotubes chemically treated with NaOH accelerated HA crystal growth in a simulated body fluid (SBF).<sup>45</sup> The kinetics of HA formation is significantly accelerated by the presence of the nanostructure associated to the NaOH treatment. In all the earlier methods, both chemical and topography changes are imparted. In this study, H<sub>2</sub>SO<sub>4</sub>/H<sub>2</sub>O<sub>2</sub> treatment removed particles from the grit-blasting process and resulted in consistent and reproducible nanoscale topography superimposed on the micron topography. Bulk chemical changes were neither induced nor observed. Many authors have presented data showing the positive effects of nanostructured surfaces on cell behavior, particularly related to osteogenesis.<sup>46–49</sup> These data cannot fully account for the superimposition of chemical changes on nanotopographic effects. However, other recent studies have shown that the size and characteristics of the features may be more important than chemical composition effects alone.<sup>50</sup>

hMSCs were used to model osteoinduction and osteoblastic differentiation in cell culture performed on three different titanium substrates. Adhesion and osteoblastic differentiation under culture conditions including osteogenic supplements occurred to varying degree on the three different surfaces. Under osteoinductive conditions, mesenchymal stem cells can reproducibly differentiate into osteoblasts when cultured on tissue culture plastic dishes.<sup>32</sup> Cooper et al.<sup>46</sup> used this model to explore the effect of titanium surface topography on adherent cell osteoblastic differentiation and showed that changes in bone matrix protein expression occur as a function of the titanium surface topography. This confirms previous observations regarding another nanoscale topography implant surface.<sup>20</sup> Recent studies using hMSCs have further demonstrated that nanotopography could influence hMSCs differentiation<sup>51,52</sup> even when no osteogenic media was added to the culture.<sup>27,53</sup> They suggested that human mesenchymal populations are especially sensitive to nanotopography and can respond by differentiation into osteoblasts. The interaction of cells with surfaces bearing nanofeatures differs from their interaction with smooth surfaces as indicated by the noted differences in filipodia formation of cells adherent to the Nano surface. Although such differences may con-

tribute to the mechanisms affecting cell responses at different surfaces, these details are beyond the scope of this investigation and have been investigated elsewhere.<sup>31,54,55</sup>

The surface-specific gene expression obtained at each time point demonstrated a relatively higher mRNA expression level for *Runx2* (3.5-fold at days 14 and 28) and *OSX* (3.5- and 4.0-fold at days 14 and 28) for Nano when compared with S and GB (Figs. 11 and 12). *Runx2* and *OSX* are key transcription factors in osteoblast differentiation,<sup>56,57</sup> and surface-dependent increase in either of their levels may be related to the differentiation observed here. *Runx2* elevations are related to increasing in the expression of other bone-related genes such as alkaline phosphatase, collagen type I, osteocalcin, and osteopontin.<sup>56,57</sup> In a study using a similar surface preparation protocol, De Oliveira and Nanci<sup>31</sup> and De Oliveira et al.<sup>40</sup> observed an early and increased expression of OPN and BSP in osteogenic cell cultures grown on nanoscale titanium surfaces when compared with control Ti. The same group also evaluated commercially available implants (MK III, Nobel Biocare, Goteborg, Sweden) treated with H<sub>2</sub>SO<sub>4</sub>/H<sub>2</sub>O<sub>2</sub>. Even though they observed an increased bone-to-implant contact in dog mandible, this treatment of commercially available implants failed in creating the nanotopography.<sup>58</sup> Increased *Runx2* and *OSX* levels have also been demonstrated in other studies with different acid etching protocol that also creates nanofeatures.<sup>20,51,59</sup> At day 7, the Gb surface presented a higher level of *OSX* mRNA relative expression that decreased rapidly to baseline levels, and the Nano surface was able to increase and maintain elevated *OSX* expression for up to 28 days. The importance of *OSX* in the surface-dependent modulation of osseointegration requires further evaluation, but initial investigation advocates the role of *OSX* in bone maturation.<sup>60</sup>

## CONCLUSION

A micron-scale grit-blasted surface imparted with nanoscale features by H<sub>2</sub>SO<sub>4</sub>/H<sub>2</sub>O<sub>2</sub> treatment affected adherent hMSCs bone-specific gene expression. These nanoscale features (<100 nm) were able to increase osteoinductive gene expression in adherent hMSCs.

## References

1. Adell R, Eriksson B, Lekholm U, Branemark PI, Jemt T. Long-term follow-up study of osseointegrated implants in the treatment of totally edentulous jaws. *Int J Oral Maxillofac Implants* 1990;5:347–359.

2. Moy PK, Medina D, Shetty V, Aghaloo TL. Dental implant failure rates and associated risk factors. *Int J Oral Maxillofac Implants* 2005;20:569–577.
3. Jaffin RA, Berman CL. The excessive loss of Branemark fixtures in type IV bone: A 5-year analysis. *J Periodontol* 1991;62:2–4.
4. Bain CA. Smoking and implant failure—Benefits of a smoking cessation protocol. *Int J Oral Maxillofac Implants* 1996; 11:756–759.
5. Fiorellini JP, Chen PK, Nevins M, Nevins ML. A retrospective study of dental implants in diabetic patients. *Int J Periodontics Restorative Dent* 2000;20:366–373.
6. Morton D, Jaffin R, Weber HP. Immediate restoration and loading of dental implants: Clinical considerations and protocols. *Int J Oral Maxillofac Implants* 2004;19 (Suppl):103–108.
7. Cooper LF. Biologic determinants of bone formation for osseointegration: Clues for future clinical improvements. *J Prosthet Dent* 1998;80:439–449.
8. Nanci A, Wuest JD, Peru L, Brunet P, Sharma V, Zalzal S, McKee MD. Chemical modification of titanium surfaces for covalent attachment of biological molecules. *J Biomed Mater Res* 1998;40:324–335.
9. Boyan BD, Schwartz Z, Hambleton JC. Response of bone and cartilage cells to biomaterials in vivo and in vitro. *J Oral Implantol* 1993;19:116–122.
10. Schwartz Z, Swain LD, Marshall T, Sela J, Gross U, Amir D, Muller-Mai C, Boyan BD. Modulation of matrix vesicle enzyme activity and phosphatidylserine content by ceramic implant materials during endosteal bone healing. *Calcif Tissue Int* 1992;51:429–437.
11. Stanford CM, Johnson GK, Fakhry A, Gratton D, Mellonig JT, Wanger W. Outcomes of a fluoride modified implant one year after loading in the posterior-maxilla when placed with the osteotome surgical technique. *Appl Osseointegr Res* 2006;5:50–55.
12. Davies JE. Understanding peri-implant endosseous healing. *J Dent Educ* 2003;67:932–949.
13. Masuda T, Salvi GE, Offenbacher S, Felton DA, Cooper LF. Cell and matrix reactions at titanium implants in surgically prepared rat tibiae. *Int J Oral Maxillofac Implants* 1997; 12:472–485.
14. Meyer U, Joos U, Mythili J, Stamm T, Hohoff A, Fillies T, Stratmann U, Wiesmann HP. Ultrastructural characterization of the implant/bone interface of immediately loaded dental implants. *Biomaterials* 2004;25:1959–1967.
15. Berglundh T, Abrahamsson I, Lang NP, Lindhe J. De novo alveolar bone formation adjacent to endosseous implants. *Clin Oral Implants Res* 2003;14:251–262.
16. Le Guéhennec L, Soueidan A, Layrolle P, Amouriq Y. Surface treatments of titanium dental implants for rapid osseointegration. *Dent Mater* 2007;23:844–854.
17. Kasemo B. Biocompatibility of titanium implants: Surface science aspects. *J Prosthet Dent* 1983;49:832–837.
18. Buser D, Schenk RK, Steinemann S, Fiorellini JP, Fox CH, Stich H. Influence of surface characteristics on bone integration of titanium implants. A histomorphometric study in miniature pigs. *J Biomed Mater Res* 1991;25:889–902.
19. Webster TJ, Schadler LS, Siegel RW, Bizios R. Mechanisms of enhanced osteoblast adhesion on nanophase alumina involve vitronectin. *Tissue Eng* 2001;7:291–301.
20. Guo J, Padilla RJ, Ambrose W, De Kok IJ, Cooper LF. Modification of TiO<sub>2</sub> grit blasted titanium implants by hydrofluoric acid treatment alters adherent osteoblast gene expression in vitro and in vivo. *Biomaterials* 2007;28:5418–5425.
21. Mendonça G, Mendonça DB, Simões LPG, Araújo AL, Leite ER, Duarte WR, Cooper LF, Aragão FJ. Nanostructured alumina-coated implant surface: Effect on osteoblast-related gene expression and bone-to-implant contact in vivo. *Int J Oral Maxillofac Implants* 2009;24:205–215.
22. Meirelles L, Currie F, Jacobsson M, Albrektsson T, Wennerberg A. The effect of chemical and nanotopographical modifications on the early stages of osseointegration. *Int J Oral Maxillofac Implants* 2008;23:641–647.
23. Mendonça G, Mendonça DB, Aragão FJ, Cooper LF. Advancing dental implant surface technology—From micron- to nanotopography. *Biomaterials* 2008;29:3822–3835.
24. Tan J, Saltzman WM. Biomaterials with hierarchically defined micro- and nanoscale structure. *Biomaterials* 2004;25:3593–3601.
25. Zinger O, Anselme K, Denzer A, Habersetzer P, Wieland M, Jeanfils J, Hardouin P, Landolt D. Time-dependent morphology and adhesion of osteoblastic cells on titanium model surfaces featuring scale-resolved topography. *Biomaterials* 2004;25:2695–2711.
26. Wieland M, Textor M, Chehroudi B, Brunette DM. Synergistic interaction of topographic features in the production of bone-like nodules on Ti surfaces by rat osteoblasts. *Biomaterials* 2005;26:1119–1130.
27. Dalby MJ, Gadegaard N, Tare R, Andar A, Riehle MO, Herzyk P, Wilkinson CD, Oreffo RO. The control of human mesenchymal cell differentiation using nanoscale symmetry and disorder. *Nat Mater* 2007;6:997–1003.
28. Vetrone F, Variola F, Tambasco de Oliveira P, Zalzal SF, Yi JH, Sam J, Bombonato-Prado KF, Sarkissian A, Perepichka DF, Wuest JD, Rosei F, Nanci A. Nanoscale oxidative patterning of metallic surfaces to modulate cell activity and fate. *Nano Lett* 2009;9:659–665.
29. Wang XX, Hayakawa S, Tsuru K, Osaka A. A comparative study of in vitro apatite deposition on heat-, H<sub>2</sub>O(2)-, and NaOH-treated titanium surfaces. *J Biomed Mater Res* 2001; 54:172–178.
30. Wang XX, Hayakawa S, Tsuru K, Osaka A. Bioactive titania-gel layers formed by chemical treatment of Ti substrate with a H<sub>2</sub>O<sub>2</sub>/HCl solution. *Biomaterials* 2002;23:1353–1357.
31. De Oliveira PT, Nanci A. Nanotexturing of titanium-based surfaces upregulates expression of bone sialoprotein and osteopontin by cultured osteogenic cells. *Biomaterials* 2004; 25:403–413.
32. Jaiswal N, Haynesworth SE, Caplan AI, Bruder SP. Osteogenic differentiation of purified, culture-expanded human mesenchymal stem cells in vitro. *J Cell Biochem* 1997;64:295–312.
33. Livak KJ, Schmittgen TD. Analysis of relative gene expression data using real-time quantitative PCR and the 2(ΔΔ–C/(T)) methods. *Methods* 2001;25:402–408.
34. Yuan JS, Reed A, Chen F, Stewart CN Jr. Statistical analysis of real-time PCR data. *BMC Bioinformatics* 2006;7:85.
35. Wescott DC, Pinkerton MN, Gaffey BJ, Beggs KT, Milne TJ, Meikle MC. Osteogenic gene expression by human periodontal ligament cells under cyclic tension. *J Dent Res* 2007;86: 1212–1216.
36. Ogawa T, Nishimura I. Different bone integration profiles of turned and acid-etched implants associated with modulated expression of extracellular matrix genes. *Int J Oral Maxillofac Implants* 2003;18:200–210.
37. Ogawa T, Nishimura I. Genes differentially expressed in titanium implant healing. *J Dent Res* 2006;85:566–570.
38. Coelho PG, Granjeiro JM, Romanos GE, Suzuki M, Silva NR, Cardaropoli G, Thompson VP, Lemons JE. Basic research methods and current trends of dental implant surfaces. *J Biomed Mater Res B: Appl Biomater* 2009;88:579–596.
39. Berglundh T, Abrahamsson I, Albouy JP, Lindhe J. Bone healing at implants with a fluoride-modified surface: An experimental study in dogs. *Clin Oral Implants Res* 2007;18:147–152.

40. De Oliveira PT, Zalzal SF, Beloti MM, Rosa AL, Nanci A. Enhancement of in vitro osteogenesis on titanium by chemically produced nanotopography. *J Biomed Mater Res A* 2007;80:554–564.
41. Puckett S, Pareta R, Webster TJ. Nano rough micron patterned titanium for directing osteoblast morphology and adhesion. *Int J Nanomed* 2008;3:229–241.
42. Uchida M, Kim HM, Miyaji F, Kokubo T, Nakamura T. Apatite formation on zirconium metal treated with aqueous NaOH. *Biomaterials* 2002;23:313–317.
43. Kim HM, Kokubo T, Fujibayashi S, Nishiguchi S, Nakamura T. Bioactive macroporous titanium surface layer on titanium substrate. *J Biomed Mater Res* 2000;52:553–557.
44. Ellingsen JE, Thomsen P, Lyngstadaas SP. Advances in dental implant materials and tissue regeneration. *Periodontol* 2000 2006;41:136–156.
45. Oh SH, Finones RR, Daraio C, Chen LH, Jin S. Growth of nano-scale hydroxyapatite using chemically treated titanium oxide nanotubes. *Biomaterials* 2005;26:4938–4943.
46. Cooper LF, Zhou Y, Takebe J, Guo J, Abron A, Holmen A, Ellingsen JE. Fluoride modification effects on osteoblast behavior and bone formation at TiO<sub>2</sub> grit-blasted c.p. titanium endosseous implants. *Biomaterials* 2006;27:926–936.
47. Webster TJ, Siegel RW, Bizios R. Osteoblast adhesion on nanophase ceramics. *Biomaterials* 1999;20:1221–1227.
48. Webster TJ, Ergun C, Doremus RH, Siegel RW, Bizios R. Enhanced functions of osteoblasts on nanophase ceramics. *Biomaterials* 2000;21:1803–1810.
49. Price RL, Gutwein LG, Kaledin L, Tepper F, Webster TJ. Osteoblast function on nanophase alumina materials: Influence of chemistry, phase, and topography. *J Biomed Mater Res A* 2003;67:1284–1293.
50. Mendes VC, Moineddin R, Davies JE. The effect of discrete calcium phosphate nanocrystals on bone-bonding to titanium surfaces. *Biomaterials* 2007;28:4748–4755.
51. Valencia S, Gretzer C, Cooper LF. Surface nanofeature effects on titanium-adherent human mesenchymal stem cells. *Int J Oral Maxillofac Implants* 2009;24:38–46.
52. Mendonça G, Mendonça DB, Simões LG, Araújo AL, Leite ER, Duarte WR, Aragão FJ, Cooper LF. The effects of implant surface nanoscale features on osteoblast-specific gene expression. *Biomaterials* 2009;30:4053–4062.
53. Dalby MJ, Andar A, Nag A, Affrossman S, Tare R, McFarlane S, Oreffo RO. Genomic expression of mesenchymal stem cells to altered nanoscale topographies. *J R Soc Interface* 2008;5: 1055–1065.
54. Dalby MJ, Gadegaard N, Riehle MO, Wilkinson CD, Curtis AS. Investigating filopodia sensing using arrays of defined nano-pits down to 35 nm diameter in size. *Int J Biochem Cell Biol* 2004;36:2005–2015.
55. Lim JY, Hansen JC, Siedlecki CA, Runt J, Donahue HJ. Human foetal osteoblastic cell response to polymer-demixed nanotopographic interfaces. *J R Soc Interface* 2005;2:97–108.
56. Harada H, Tagashira S, Fujiwara M, Ogawa S, Katsumata T, Yamaguchi A, Komori T, Nakatsuka M. Cbfa1 isoforms exert functional differences in osteoblast differentiation. *J Biol Chem* 1999;274:6972–6978.
57. Harada S, Rodan GA. Control of osteoblast function and regulation of bone mass. *Nature* 2003;423:349–355.
58. Tavares MG, de Oliveira PT, Nanci A, Hawthorne AC, Rosa AL, Xavier SP. Treatment of a commercial, machined surface titanium implant with H<sub>2</sub>SO<sub>4</sub>/H<sub>2</sub>O<sub>2</sub> enhances contact osteogenesis. *Clin Oral Implants Res* 2007;18:452–458.
59. Isa ZM, Schneider GB, Zaharias R, Seabold D, Stanford CM. Effects of fluoridemodified titanium surfaces on osteoblast proliferation and gene expression. *Int J Oral Maxillofac Implants* 2006;21:203–211.
60. Baek WY, Lee MA, Jung JW, Kim SY, Akiyama H, de Crombrughe B, Kim JE. Positive regulation of adult bone formation by osteoblast-specific transcription factor osterix. *J Bone Miner Res* 2009;24:1055–1065.